Revue Paralia, Volume 11 (2018) pp n01.15-n01.28
Keywords: Nonlinear waves, Coastal hydrodynamics, Water wave simulation, Numerical modeling, Wave models, Radial Basis Functions.

Development of a nonlinear and dispersive numerical model of wave propagation in the coastal zone

Cécile RAOULT [1,2], Michel BENOIT [3], Marissa L. YATES [1,4]

1. Laboratoire d'Hydraulique Saint-Venant, Université Paris-Est, Unité de recherche commune EDF R&D, Cerema, Ecole de Ponts ParisTech, 6 quai Watier, BP 49, 78401 Chatou cedex, France.
2. EDF R&D, Laboratoire National d'Hydraulique et Environnement – LNHE, 6 quai Watier, BP 49, F-78401 Chatou cedex, France.
3. Aix-Marseille Université, Institut de Recherche sur les Phénomènes Hors-Equilibre (IRPHE), UMR 7342- CNRS, Aix-Marseille Université, Ecole Centrale Marseille, 49 rue Frédéric Joliot-Curie, BP 146, F-13384 Marseille Cedex 13, France.
4. Cerema, Division technique Eau, mer et fleuves, 134 rue de Beauvais, 60280 Margny-les-Compiègne, France.
cecile.raoult@edf.fr ; benoit@irphe.univ-mrs.fr ; marissa.yates-michelin@cerema.fr

Abstract:
Nonlinear and dispersive effects are significant for nearshore waves, leading to the study and development of a fully nonlinear and dispersive potential-flow model solving the Euler-Zakharov equations, which determine the temporal evolution of the free surface elevation and velocity potential.
The mathematical model and its numerical implementation are presented, as well as the approach chosen to extend the model to two horizontal dimensions. The nonlinear and dispersive capabilities of the 1DH version of the model are demonstrated by applying the model to two test cases: (1) the generation of regular waves created by a piston-like wave maker and the propagation of the associated free and bound harmonics over a flat bottom, following the experiments of CHAPALAIN *et al.* (1992), and (2) the propagation of irregular waves over a barred beach profile, following the experiments of BECQ-GIRARD *et al.* (1999). The accuracy of the model in representing high-order nonlinear and dispersive effects is demonstrated by the reproduction of the energy transfers between different harmonic components.

Paper selected during the colloquium "XIVèmes Journées Nationales Génie Côtier Génie Civil", Toulon (France), 29 June to 1st July 2016.
Received 9 January 2017, accepted 16 May 2018, available online 18 June 2018.
Translated version not certified, published under the responsibility of the authors.

How to cite the original paper:
RAOULT C., BENOIT M., YATES M.L. (2018). Développement d'un modèle numérique non-linéaire et dispersif pour la propagation des vagues en zone côtière. Revue Paralia, Vol. 11, pp n01.1–n01.14.
DOI: https://doi.org/10.5150/revue-paralia.2018.n01

Then, the development of the 2DH version of the model is tested simulating the propagation of regular waves over a semi-circular step acting as a converging lens, reproducing two experiments of WHALIN (1971). The initial results obtained using Radial Basis Functions to estimate the horizontal derivatives demonstrate the ability of the model to simulate wave propagation over variable 2DH bathymetries. These results indicate the potential of applying the model to simulate realistic cases.

1. Introduction

Wave transformation from the offshore to the beach includes a variety of different physical processes from refraction and shoaling, to dissipation due to bottom friction or wave breaking, diffraction, reflection from structures, islands or shoals, etc. Accurate simulation of all of these processes is not an easy task, especially given the significant variation of the relative water depth $\mu = kh$ (where k is the wave number and h is the water depth) between the offshore and the coast. Furthermore, nonlinear effects, quantified by the steepness parameter $\varepsilon = kH/2$ or the relative wave height H/h (where H is a characteristic wave height) become important in the coastal zone because of the decrease in water depth.

To represent accurately these two effects, numerical models of wave propagation require high nonlinear and dispersive capabilities. In the field of coastal and harbor engineering, some frequently used modeling approaches are based on the mild-slope equation of BERKHOFF (1972) or one of its extensions, which neglect nonlinear effects. Other models resolving the Boussinesq, Serre or Green-Naghdi equations take into account some of the nonlinear and dispersive effects (*e.g.* MADSEN *et al*., 1991 ; NWOGU, 1993 ; KIRBY, 2003 ; CHAZEL *et al*., 2011). However, these models are only partially nonlinear and/or dispersive, even when using high-order formulations (MADSEN *et al.*, 2002, 2006; BENOIT & CHAZEL, 2013).

With the objective of obtaining a highly accurate simulation tool, a fully nonlinear and dispersive model is developed, based on the Euler-Zakharov equations (ZAKHAROV, 1968) by assuming potential flow theory (YATES & BENOIT, 2015). BENOIT *et al.* (2014) and RAOULT *et al*. (2014, 2016) presented several validation test cases of the 1DH (*x,z*) version of the code for non-breaking waves. Here, the recent developments and validation are presented and discussed.

The bases of the mathematical model are briefly outlined in part 2, then the numerical implementation is presented in part 3. In part 4, the simulation results from the 1DH model are compared to two sets of experimental measurements where strong nonlinear effects are observed. A preliminary application to a 2DH (*i.e.* 3D) test case is presented in part 5. This test case simulates the experiments of WHALIN (1971) for two incident wave conditions propagating over a bathymetric profile causing wave convergence. Conclusions and perspectives are summarized in part 6.

2. Presentation of the mathematical model

Assuming irrotational flow of an inviscid fluid with constant density, the potential flow approach is adopted. The fluid system is described by the velocity potential $\Phi(\vec{x},z,t)$, with $\vec{x}=(x,y)$, satisfying the Laplace equation in the entire domain (mass conservation). The Laplace equation is supplemented by the kinematic and dynamic nonlinear boundary conditions at the free surface, $z=\eta(\vec{x},t)$, an impermeable condition at the bottom $z=-h(\vec{x},t)$, and Dirichlet or Neumann conditions at the lateral boundaries. For the applications presented here, the bathymetric profile is constant in time, but the model may be used to study tsunami-like cases with the generation of waves by a moving bottom (see BENOIT *et al.* 2014).

By assuming the continuity of the water column between the bottom and the free surface, the velocity potential at the free surface $\Psi(\vec{x},t)= \Phi(\vec{x},z=\eta(\vec{x},t),t)$ can be defined. The free surface boundary conditions become (ZAKHAROV, 1968):

$$\frac{\partial \eta}{\partial t} = -\nabla\eta.\nabla\Psi + \tilde{w}\left(1+(\nabla\eta)^2\right) \tag{1}$$

$$\frac{\partial \Psi}{\partial t} = -g\eta - \frac{1}{2}(\nabla\Psi)^2 + \frac{1}{2}\tilde{w}^2\left(1+(\nabla\eta)^2\right) \tag{2}$$

where $\tilde{w}(\vec{x},t) \equiv \frac{\partial \Phi}{\partial z}(\vec{x},z=\eta,t)$ is the vertical component of the free surface velocity.

This set of equations (1-2) is expressed only as a function of surface quantities. However, the temporal integration of these equations requires calculating $\tilde{w}$, which must be estimated from η and ψ, a problem called "Dirichlet-to-Neumann" (DtN).

3. Presentation of the numerical implementation

The numerical resolution of equations (1-2) requires: a temporal integration scheme, a method to solve the DtN problem, and an approach to compute the first and second-order spatial derivatives. Details on the numerical implementation of the 1DH (x,z) version of the model are available in YATES & BENOIT (2015) and RAOULT *et al.* (2014, 2016); only the main elements are repeated here. To integrate in time, an explicit fourth-order Runge-Kutta scheme with a constant time step is used.

The DtN problem is solved using a spectral approach in the vertical (TIAN & SATO, 2008) to obtain the solution of the Laplace boundary value problem for the velocity potential Φ in the entire domain. A change in the vertical coordinate defined by:

$$s(\vec{x},z,t) = \frac{2z + h(\vec{x},t) - \eta(\vec{x},t)}{h(\vec{x},t) + \eta(\vec{x},t)} \tag{3}$$

transforms the irregularly shaped domain to a domain of constant height, with $s=-1$ at the bottom and $s=+1$ at the free surface. Then, the velocity potential is approximated with a spectral approach, using a basis of Chebyshev polynomials of the first kind $T_n(s)$ over the range $[-1,+1]$:

$$\Phi(\vec{x},z,t)=\varphi(\vec{x},s(\vec{x},z,t),t)\approx\sum_{n=0}^{N_T}a_n(\vec{x},t)\,T_n(s). \tag{4}$$

The expansion is truncated at order N_T. For practical applications, the optimal value appears to be between 5 and 10, as shown by BENOIT *et al.* (2014) and RAOULT *et al*. (2014, 2016). In the 1DH version of the model, fourth-order finite difference schemes are used to estimate the horizontal spatial derivatives, allowing variable spatial resolution for general cases. In practice, the resolution of the Laplace boundary value problem at a given time results in the resolution of a linear system for the $a_n(\vec{x})$ coefficients for $n=0,1,\dots,N_T$. The vertical velocity at the free surface is then given by:

$$\tilde{w}(\vec{x},t)=\frac{\partial\Phi}{\partial z}(\vec{x},z=\eta,t)=\frac{\partial s}{\partial z}\frac{\partial\varphi}{\partial s}(\vec{x},s=1,t)\approx\frac{2}{h(\vec{x},t)+\eta(\vec{x},t)}\sum_{n=1}^{N_T}n^2a_n(\vec{x},t) \tag{5}$$

In order to simulate realistic test cases with complex bathymetric profiles and waves, the model was extended to two horizontal dimensions (*i.e.* 3D). To maintain the flexibility of the approach and to apply the model to irregularly shaped domains, the horizontal plane is discretized with scattered nodes, and the horizontal derivatives are estimated using the Radial Basis Function (RBF) method (WRIGHT & FORNBERG, 2006). The spectral approach in the vertical dimension is maintained. The derivative of a function *f* at node $\overrightarrow{x_l}$ is approximated by a linear combination of the values of the function *f* at the *n*-1 nearest neighbors (*n* is the number of nodes in the stencil):

$$L(f)(\overrightarrow{x_l})=\sum_{k=1}^{n}w_{l,k}^{L}\,f(\overrightarrow{x_k}) \tag{6}$$

with *L* any linear differential operator and the $w_{l,k}^{L}$ the unknown coefficients to be determined for each operator *L* at each node $\overrightarrow{x_l}$. To achieve this, a set of test functions forming a base is chosen, for which the approximation must be satisfied. Here, radial functions are considered, centered at the nodes of the stencil $\overrightarrow{x_k}$ $_{k=1,n}$: $\varphi_k(\vec{x})=\Phi(\|\overrightarrow{x}-\overrightarrow{x_k}\|)$. This leads to the resolution of a linear set of *n* equations for *n* unknowns, which can be written as:

$$\begin{bmatrix}\Phi(\|\overrightarrow{x_1}-\overrightarrow{x_1}\|) & \Phi(\|\overrightarrow{x_2}-\overrightarrow{x_1}\|) & \dots & \Phi(\|\overrightarrow{x_n}-\overrightarrow{x_1}\|)\\ \Phi(\|\overrightarrow{x_1}-\overrightarrow{x_2}\|) & \Phi(\|\overrightarrow{x_2}-\overrightarrow{x_2}\|) & & \vdots\\ \vdots & & \ddots & \vdots\\ \Phi(\|\overrightarrow{x_1}-\overrightarrow{x_n}\|) & \dots & \dots & \Phi(\|\overrightarrow{x_n}-\overrightarrow{x_n}\|)\end{bmatrix}\begin{bmatrix}w_{l,1}^{L}\\ w_{l,2}^{L}\\ \vdots\\ w_{l,n}^{L}\end{bmatrix}=\begin{bmatrix}L\Phi(\|\overrightarrow{x}-\overrightarrow{x_1}\|)(\overrightarrow{x_l})\\ L\Phi(\|\overrightarrow{x}-\overrightarrow{x_2}\|)(\overrightarrow{x_l})\\ \vdots\\ L\Phi(\|\overrightarrow{x}-\overrightarrow{x_n}\|)(\overrightarrow{x_l})\end{bmatrix} \tag{7}$$

With fixed nodes, this set of equations is solved only once at the beginning of the simulation for each differential operator at every node in the domain. In the following, the multiquadric radial function (WRIGHT & FORNBERG, 2006) is used:

$$\Phi(\|\overrightarrow{x}-\overrightarrow{x_k}\|)=\sqrt{\|\overrightarrow{x}-\overrightarrow{x_k}\|^2+c^2} \tag{8}$$

where c is a shape parameter. This parameter controls the flatness of the function. The larger the value of c, the flatter the function. Increasing the value of c tends to reduce the approximation error but may also increase the condition number of the matrix and lead to larger numerical errors in the resolution of the system.

4. Validation of the 1DH version of the model

4.1 Dynamics of regular waves generated by a piston-type wave-maker over a flat bottom

CHAPALAIN *et al*. (1992) studied the propagation over a flat bottom of waves generated by the sinusoidal motion of a piston-type wave-maker. This test case consists of reproducing trial A of the experiments corresponding to a sinusoidal motion with a maximum amplitude e=7.8 cm and period T=2.5 s, in a water depth h=0.4 m. From the linear dispersion relation, the wavelength is estimated as L=4.74 m. In the simulations, a vertically uniform velocity profile that varies sinusoidally in time, is applied at the left boundary. The right boundary is located far enough from the wave maker to avoid reflections. Waves are propagated during 16 wave periods (approximately 40 s) with a time step $\Delta t=T/40=0.0625$ s. The maximum order of the Chebyshev polynomial is N_T=7, and a regular mesh is used with Δx=0.1 m.

Once the stationary state is reached, a Fourier analysis of the free surface elevation time series is completed to estimate the amplitudes and phases of the harmonics (Figure 1a). The model simulates accurately the transfer of energy between the different harmonics, reproducing well the beat length, induced by the co-existence of free and bound waves of the 2nd, 3rd, and 4th harmonics. The slight overestimation of the amplitude of the second harmonic ($2f$) by the model after x=19 m, is likely explained by the fact that dissipative effects are not taken into account in the simulations. The spatial evolution of the phase difference between the first and second harmonic (Figure 1b), is well represented by the model, oscillating between $-\pi/2$ and $+\pi/2$ with the same beat length as that observed in the spatial evolution of the amplitude. The two first harmonics are in phase when the first harmonic amplitude is maximum and the second harmonic amplitude is minimum, and *vice versa*.

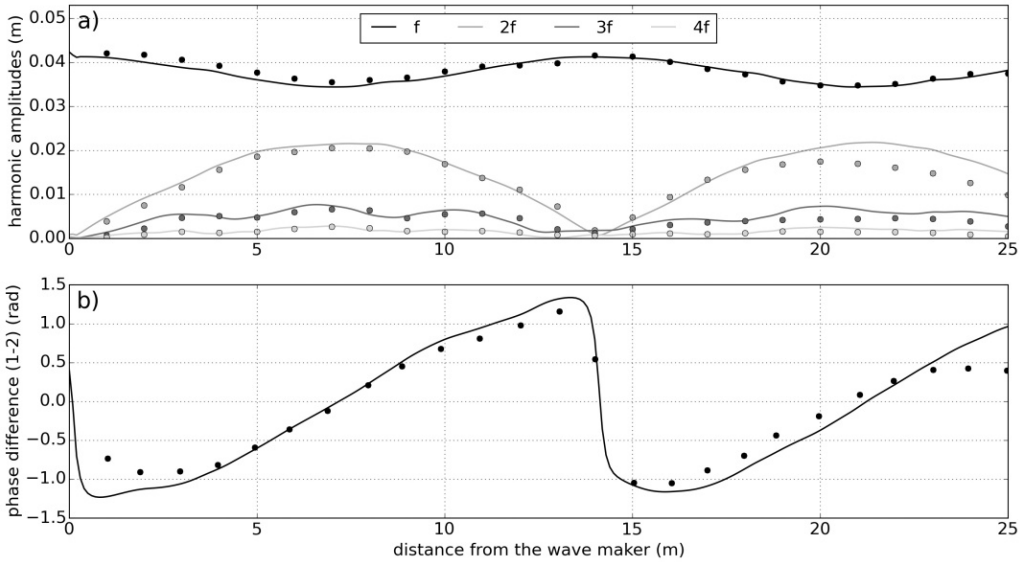

Figure 1. Spatial evolution a) of the first four harmonic amplitudes of the free surface elevation for trial A of CHAPALAIN et al. (1992) and b) of the phase difference between the first and second harmonic. The experimental results are represented by the dots and the simulation results are represented by the solid lines.

4.2 Propagation of irregular waves over a submerged bar

This test case simulates the propagation of irregular waves over a submerged bar following the experiments of BECQ-GIRARD *et al*. (1999). The bathymetric profile (Figure 2) was designed to study nonlinear effects in shallow water. In the experiments, irregular waves are generated using a JONSWAP wave spectrum with a peak enhancement factor of γ=3.3, a peak period T_p=2.39 s, and a significant wave height H_{m0}=3.4 cm in the deep end of the wave flume where h=0.65 m (trial 26 of BECQ-GIRARD *et al*. (1999), without wave breaking). The free surface elevation is measured at 16 probes during 40 min with a time step Δt=0.07 s.

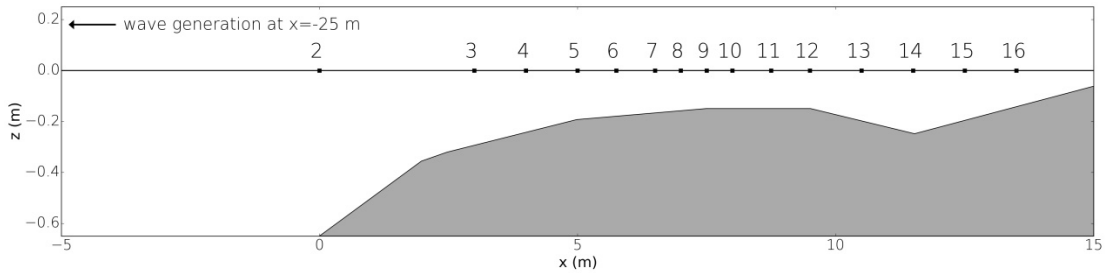

Figure 2. Bathymetric profile and location of the wave measurement probes for the experiments of BECQ-GIRARD et al. (1999).

For the simulations, the computational domain extends from x=−5 m to +25 m, with the foot of the bar located at x=0 m. The horizontal domain is discretized regularly with a

resolution of Δx=0.05 m, and N_T=7. The free surface elevation measured at probe 2 is used to force the model. The associated velocity potential is reconstructed from a spectral analysis of the time series using linear theory and then imposed at the left boundary. A 5 m-long relaxation zone is added for wave generation, where the free surface elevation and velocity potential are corrected at the end of each time step. At the right side of the domain, a 10 m-long relaxation zone is added to absorb waves. The waves propagate during 2380 s (approximately 39.7 min) with a time step equivalent to the sampling frequency of the probes.

The free surface variance spectra calculated from the simulation results agree well with those calculated from the measurements (e.g. Figure 3, probes 2, 9, 15, and 16). The transfer of energy from the main peak (at frequency f_p) to higher frequencies is observed with the appearance of peaks at the harmonic frequencies (up to the fifth harmonic) in the spectrum of probe 9. After the bar, as the water depth increases, the energy transfer reverses, with most of the energy returning to the second harmonic. Spectral peaks at the third, fourth, and fifth harmonics disappear at probe 15, while the peak of the second harmonic increases. Finally, a peak at the third harmonic reappears at probe 16 due to the decrease in water depth at the end of the bathymetric profile. The evolution of the low frequency part of the spectrum is also represented well by the model.

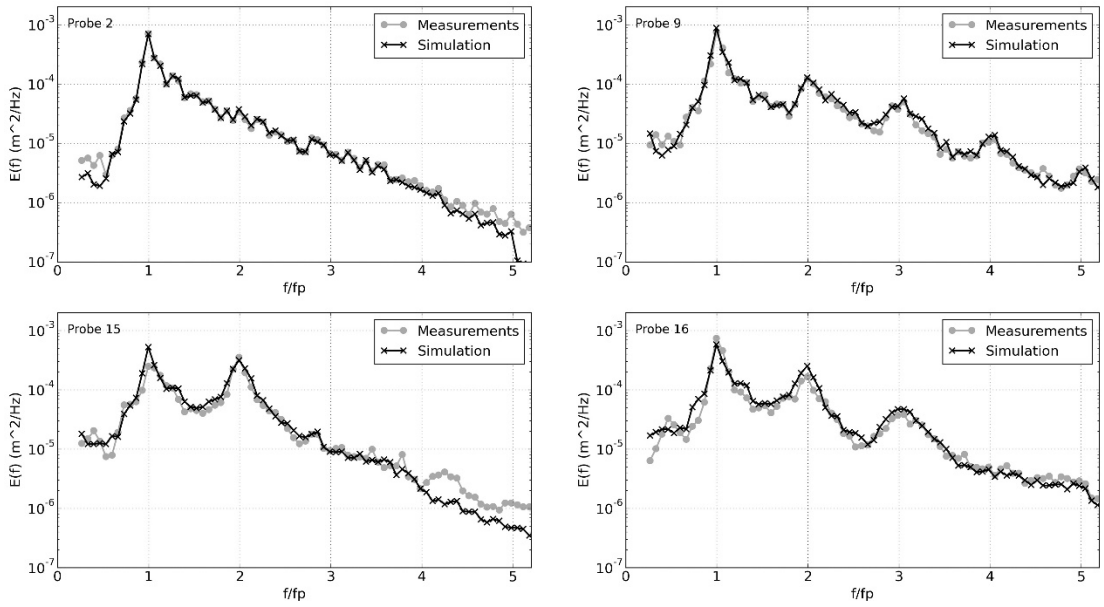

Figure 3. Comparison of the variance spectra computed from the free surface elevation measured (gray) and simulated (black) at four probes (2, 9, 15 and 16) for trial 26 of the experiments of BECQ-GIRARD et al. (1999).

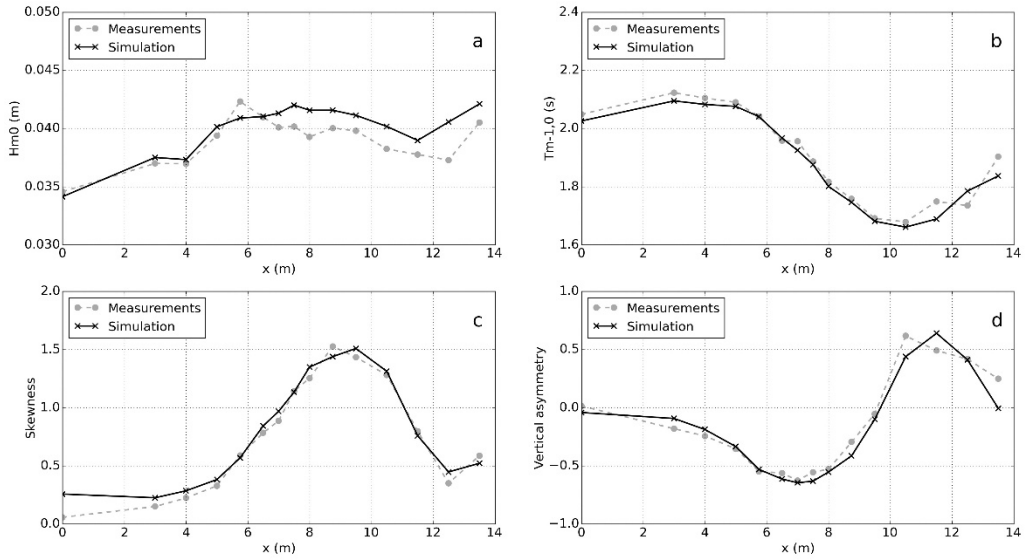

Figure 4. Comparison of integral parameters of the sea state measured (gray) and simulated (black) along the bathymetric profile of the experiments of BECQ-GIRARD et al. (1999): a) significant wave height, b) mean period, c) skewness (horizontal asymmetry) and d) vertical asymmetry.

The model represents accurately the spatial evolution of integral wave parameters such as the significant wave height H_{m0} (Figure 4a) and the mean period $T_{m-1,0}$ (Figure 4b), computed from moments of the variance spectrum. Nonlinear effects appear as an increase in the significant wave height due to shoaling as the water depth decreases, followed by a decrease in the significant wave height over the trough. The mean period first decreases because of the transfer of energy from low to high frequencies and then increases when this transfer reverses. Moreover, two parameters quantifying the wave asymmetry were studied: the skewness (Figure 4c) and the vertical asymmetry (Figure 4d), defined respectively as:

$$\lambda_3 = \frac{\left\langle \left(\eta - \langle\eta\rangle\right)^3 \right\rangle}{m_o^{3/2}} = \frac{\sum_{m=-\infty}^{+\infty}\sum_{n=-\infty}^{+\infty} \mathrm{Re}\left[B_{m,n}\right]}{m_o^{3/2}} \qquad A = \frac{\sum_{m=-\infty}^{+\infty}\sum_{n=-\infty}^{+\infty} \mathrm{Im}\left[B_{m,n}\right]}{m_o^{3/2}} \tag{9}$$

where $B_{m,n} = B(f_m, f_n)$ is the bispectrum, or Fourier transform of the third-order autocorrelation function of the free surface elevation. These two parameters account for the asymmetry between the crest and trough elevation and between the front and back faces of the wave, respectively. In the deepest part of the bathymetric profile, the waves are weakly nonlinear, and these parameters are close to zero. The skewness and vertical asymmetry evolve along the bathymetric profile showing good agreement between the simulations and the measurements as the wave profiles become asymmetric with respect to the horizontal and vertical planes.

5. Application and validation of the 2DH version of the model

This test case, based on the experiments of WHALIN (1971), consists in propagating regular waves over a semi-circular step acting as a focusing lens for the waves (Figure 5.a). In the experiments, regular waves are generated by a piston-type wave-maker in a 25.63 m-long and 6.096 m-wide wave tank, with a water depth of 0.4572 m. The bathymetric profile used in the simulations is the one described by SHAO & FALTINSEN (2014). Two incident wave conditions are simulated. The first case corresponds to regular waves with a period T=2 s and an amplitude a=0.0075 m. For the second case, the wave period is the same, but the amplitude increases to a=0.0106 m. The associated velocity potential is imposed at the left boundary. The computational domain contains the zone of interest between 0 and 25 m, which is supplemented by two relaxation zones: (1) a 3.91 m-long relaxation zone (*i.e.* one wavelength) at the left boundary to absorb waves reflected from the step and to reduce the reflections from this boundary, and (2) a 7.5 m-long relaxation zone (*i.e.* three wavelengths) at the right boundary to absorb waves. Impermeable boundary conditions are applied at the lateral boundaries. The domain is discretized by 60,716 scattered nodes (spaced approximately 0.06 m apart). Waves are propagated during 36 s (*i.e.* 18 periods) with a time step $\Delta t = T/75 = 0.0267$ s. Stencils with n=13 nodes are used (*i.e.* the stencil of each node consists of the node and its 12 nearest neighbors), and the shape parameter is set to c=1, based on sensitivity tests of the accuracy of the results as a function of these two parameters.

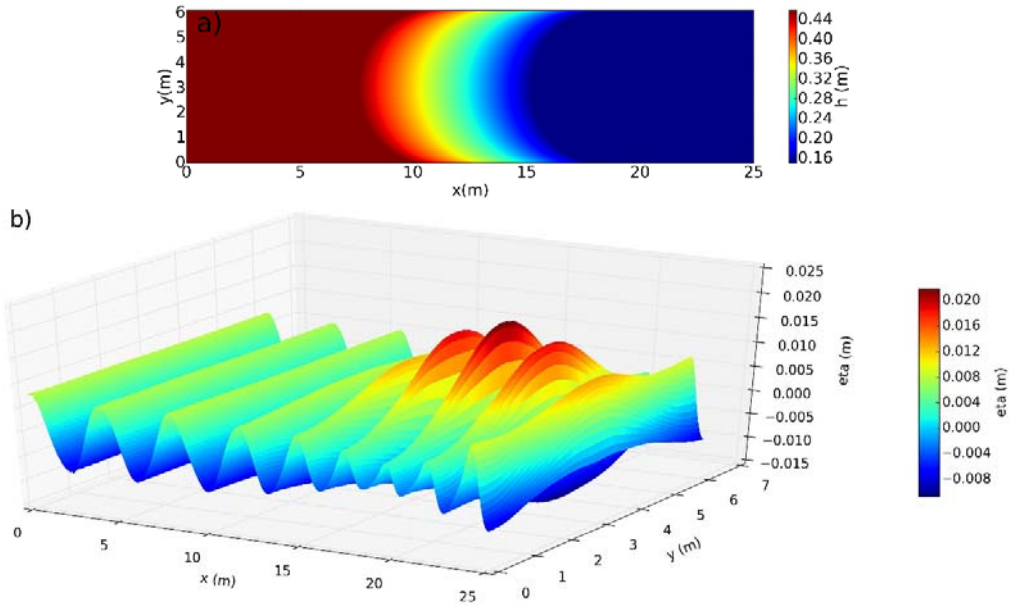

Figure 5. (a) Bathymetry and (b) simulated free surface elevation at the end of the simulation (t≈36.045s) for the experiments of WHALIN (1971) with T=2 s and a=0.0075 m.

The free surface elevation at the end of the simulation in the first case (Figure 5b) shows that, in the deeper part of the domain before the slope, waves are nearly sinusoidal and uniform in the *y*-direction. When the waves propagate over the slope, the wave field becomes three dimensional with highly nonlinear effects. The increase of the free surface elevation in the shallower zone is due to a combination of the effects of shoaling, diffraction, and refraction induced by the bathymetric profile. A Fourier analysis of the free surface elevation time series along the central axis of the tank shows the spatial evolution of the first three harmonics (Figure 6, for a=0.0075 m). The simulation results compare well with the experimental data. The second harmonic amplitude is slightly under estimated in the deeper part of the domain (x<10 m), likely because waves are generated using linear wave theory in the code. In the convergence zone (x≈20 m), the evolution of the harmonic amplitudes is reproduced well, in particular the increase of the second (2f) and third (3f) harmonic amplitudes due to transfers of energy from the first harmonic. Despite these energy transfers, the first harmonic amplitude remains constant after the step (outside of the absorption zone). This interesting observation can be explained by the fact that refraction effects induced by the bathymetric profile focus energy at a rate that is sufficient to compensate for the transfers of energy to higher order harmonics. For the second simulated case, with a larger incident wave height, the nonlinear effects are even more significant (Figure 7, for a=0.0106 m). In the convergence zone, the amplitude of the second harmonic reaches approximately two-thirds of the amplitude of the first harmonic, whereas in the first case it reached only one half. The transfer of energy from the first to the higher harmonics is no longer fully compensated for by refraction effects, and the amplitude of the first harmonic therefore decreases around x=20 m.

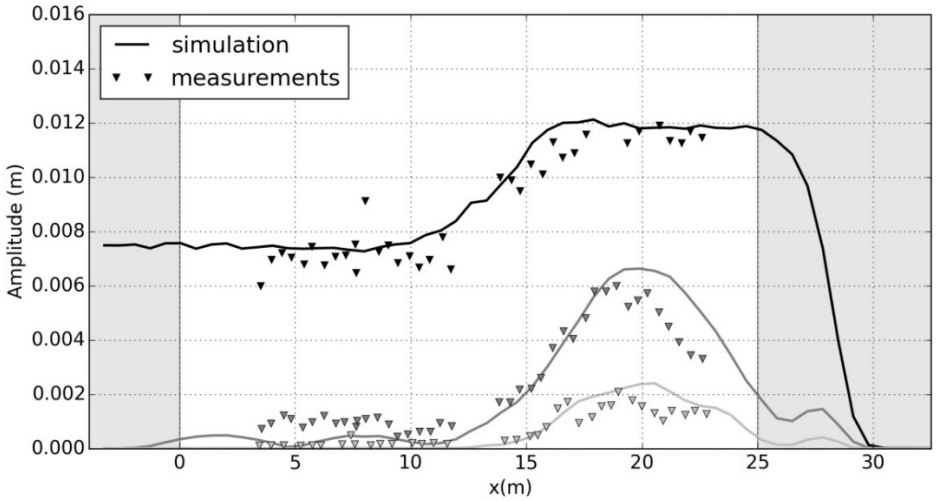

Figure 6. Spatial evolution of the first three harmonic amplitudes for the first case of WHALIN (1971), with T=2 s and a=0.0075 m. The shaded gray areas correspond to the relaxation zones used in the numerical model, and the three colors correspond to first (black), second (dark gray), and third (light gray) harmonics.

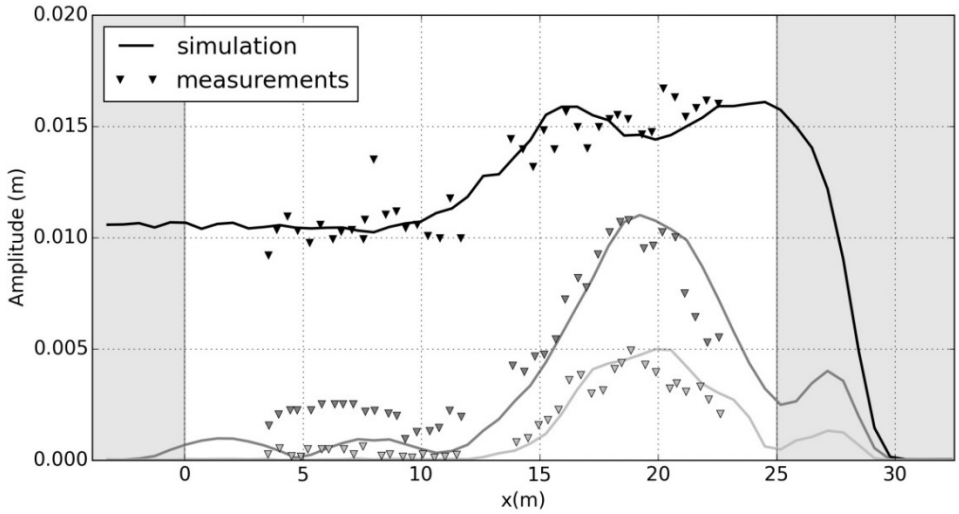

Figure 7. Spatial evolution of the first three harmonic amplitudes for the second case of WHALIN (1971), with T=2 s and a=0.0106 m. The shaded gray areas correspond to the relaxation zones used in the numerical model, and the three colors correspond to first (black), second (dark gray), and third (light gray) harmonics.

This test case demonstrates the ability of the model to simulate accurately strong nonlinear effects (refraction and shoaling) for a convergent 3D bathymetric profile.

6. Conclusions and perspectives

Based on a nonlinear potential flow approach (Euler-Zakharov equations), the proposed numerical model is applied to simulate the transformation of nearshore waves, including

nonlinear and dispersive effects, for a wide range of relative water depths. The two 1DH test cases confirm the nonlinear and dispersive capacities of the model, in particular the transfers of energy between the different harmonics (free or bound waves) during their generation and propagation. The beat lengths of the second and third harmonics observed in the experiments of CHAPALAIN *et al*. (1992) are reproduced well by the model. When simulating the transformation of irregular waves over a realistic coastal bathymetric profile (BECQ-GIRARD *et al.*, 1999), the model is able to represent accurately the evolution of the spectral harmonic peaks up to the fifth harmonic.

In addition, the use of Radial Basis Functions (RBF) to extend the model to two horizontal dimensions was verified, showing the accurate representation of nonlinear effects observed in the experiments of WHALIN (1971), for two different wave amplitudes. This set of experiments used a semi-circular bathymetric profile causing wave energy convergence along the central axis of the tank, with strong nonlinear effects, caused by refraction and shoaling. Two advantages of the RBF method are its capacity to handle irregularly scattered nodes and its flexibility allowing the local refinement of nodes for real applications.

Determining the optimal value of the shape parameter used in the multiquadric function may, however, require a significant number of tests. Other radial functions that do not depend on a shape parameter (*e.g.* BARNETT, 2015) currently are being tested to validate the 2DH version of the model. In addition, future work will focus on including the effects of dissipation induced by wave breaking and the implementation of a run-up boundary condition for sloping bottoms. The parallelization of 2DH version of the model also should be completed to optimize the code for coastal and harbor engineering applications.

7. References

BARNETT G.A. (2015) *A robust RBF-FD formulation based on polyharmonic splines and polynomials*. PhD Thesis, University of Colorado.

BECQ-GIRARD F., FORGET P., BENOIT M. (1999) *Non-linear propagation of unidirectional wave fields over varying topography*. Coastal Engineering, Vol. 38, pp 91-113. https://doi.org/10.1016/S0378-3839(99)00043-5

BENOIT M., CHAZEL F. (2013). *Validation expérimentale d'un modèle double-couche pour des vagues côtières non-linéaires et fortement dispersives*. Revue Paralia, Vol. 6, pp 7.1–7.16. https://doi.org/10.5150/revue-paralia.2013.007

BENOIT M., RAOULT C., YATES M.L. (2014) *Fully nonlinear and dispersive modelling of surf zone waves: non-breaking tests.* Coastal Engineering Proceedings, 1(34), waves.15, 15-20 July 2014, Seoul (Korea). https://doi.org/10.9753/icce.v34.waves.15

BERKHOFF J.C.W. (1972) *Computation of combined refraction–diffraction.* Proceeding of the 13th International Conference on Coastal Engineering, ASCE, Vancouver (Canada), pp 470-490.

CHAPALAIN G., COINTE R., TEMPERVILLE A. (1992) *Observed and modeled resonantly interacting progressive water-waves*. Coastal Engineering, Vol. 16, pp 267-300. https://doi.org/10.1016/0378-3839(92)90045-V

CHAZEL F., LANNES D., MARCHE F. (2011). *Numerical simulation of strongly nonlinear and dispersive waves using a Green–Naghdi model*. Journal of Scientific Computing, Vol. 48(1-3), pp 105–116. https://doi.org/10.1007/s10915-010-9395-9

KIRBY J.T. (2003). *Boussinesq models and applications to nearshore wave propagation, surf zone processes and wave-induced currents*. Advances in Coastal Modeling, V.C. Lakhan (ed), Elsevier, pp 1–41.

MADSEN P.A., MURRAY R., SORENSEN O.R. (1991). *A new form of the Boussinesq equations with improved linear dispersion characteristics*. Coastal Engineering, Vol. 15, pp 371–388. https://doi.org/10.1016/0378-3839(91)90017-B

MADSEN P.A., BINGHAM H.B., LIU H. (2002). *A new Boussinesq method for fully nonlinear waves from shallow to deep water*. Journal of Fluid Mechanics, Vol. 462, pp 1–30. https://doi.org/10.1017/S0022112002008467

MADSEN P.A., FUHRMAN D.R., WANG B. (2006). *A Boussinesq-type method for fully nonlinear waves interacting with a rapidly varying bathymetry*. Coastal Engineering, Vol. 53, pp 487–504. https://doi.org/10.1016/j.coastaleng.2005.11.002

NWOGU O.G. (1993). *Alternative form of Boussinesq equations for nearshore wave propagation*. Journal of Waterway, Port, Coastal and Ocean Engineering, Vol. 119, pp 618–638. https://doi.org/10.1061/(ASCE)0733-950X(1993)119:6(618)

RAOULT C., BENOIT M., YATES M.L. (2014) *Etude et qualification d'un modèle numérique complètement non-linéaire et dispersif pour les vagues en zone côtière*. XIIIème Journées Nationales Génie Côtier Génie Civil, 2-4 juillet 2014, Dunkerque (France), pp 159-168. https://doi.org/10.5150/jngcgc.2014.018

RAOULT C., BENOIT M., YATES M.L. (2016) *Validation of a fully nonlinear and dispersive wave model with laboratory non-breaking experiments*. Coastal Engineering, Vol. 114, pp 194–207. https://doi.org/10.1016/j.coastaleng.2016.04.003

SHAO Y-L., FALTINSEN O.M. (2014) *A harmonic polynomial cell (HPC) method for 3D Laplace equation with application in marine hydrodynamics*. Journal of Computational Physics, Vol. 274, pp 312-332. https://doi.org/10.1016/j.jcp.2014.06.021

TIAN Y., SATO S. (2008). *A numerical model on the interaction between nearshore nonlinear waves and strong currents*. Coastal Engineering Journal, Vol. 50(4), pp 369–395. https://doi.org/10.1142/S0578563408001879

WHALIN R.W. (1971) *The limit of applicability of linear wave refraction theory in a convergence zone*. Technical report, DTIC Documents.

WRIGHT G.B., FORNBERG B. (2006) *Scattered node compact finite difference-type formulas generated from radial basis functions*. Journal of Computational Physics, Vol. 212, pp 99-123. https://doi.org/10.1016/j.jcp.2005.05.030

YATES M.L., BENOIT M. (2015) *Accuracy and efficiency of two numerical methods of solving the potential flow problem for highly nonlinear and dispersive water waves.* International Journal for Numerical Methods in Fluids. Vol. 77(10), pp 616-640. https://doi.org/10.1002/fld.3992

ZAKHAROV V.E. (1968). *Stability of periodic waves of finite amplitude on the surface of a deep fluid*. Journal of Applied Mechanics and Technical Physics, Vol. 9(2), pp 190–194. https://doi.org/10.1007/BF00913182